Ca^{2+} sparks and secretion in dorsal root ganglion neurons

Kunfu Ouyang*[†‡], Hui Zheng*[‡§], Xiaomei Qin[¶], Chen Zhang*[§], Dongmei Yang*[†], Xian Wang[¶], Caihong Wu*[†], Zhuan Zhou*[†§‖], and Heping Cheng*[‖**]

*Institute of Molecular Medicine and †National Laboratory of Biomembrane and Membrane Biotechnology, Peking University, Beijing, China; §Institute of Neuroscience, Shanghai Institutes for Biological Sciences, Chinese Academy of Sciences, Shanghai 200031, China; ¶Department of Physiology, Health Science Center, Peking University, Beijing 100083, China; and **Laboratory of Cardiovascular Sciences, National Institute on Aging, National Institutes of Health, Bethesda, MD 20892

Ca^{2+} sparks as the elementary intracellular Ca^{2+} release events are instrumental to local control of Ca^{2+} signaling in many types of cells. Here, we visualized neural Ca^{2+} sparks in dorsal root ganglion (DRG) sensory neurons and investigated possible role of DRG sparks in the regulation of secretion from the somata of the cell. DRG sparks arose mainly from type 3 ryanodine receptor Ca^{2+} release channels on subsurface cisternae of the endoplasmic reticulum, rendering a striking subsurface localization. Caffeine- or 3,7-dimethyl-1-(2-propynyl)xanthine-induced store Ca^{2+} release, in the form of Ca^{2+} sparks, triggered exocytosis, independently of membrane depolarization and external Ca^{2+}. The spark–secretion coupling probability was estimated to be between 1 vesicle per 6.6 sparks and 1 vesicle per 11.4 sparks. During excitation, subsurface sparks were evoked by physiological Ca^{2+} entry via the Ca^{2+}-induced Ca^{2+} release mechanism, and their synergistic interaction with Ca^{2+} influx accounted for ≈60% of the Ca^{2+}-dependent exocytosis. Furthermore, inhibition of Ca^{2+}-induced Ca^{2+} release abolished endotoxin-induced secretion of pain-related neuropeptides. These findings underscore an important role for Ca^{2+} sparks in the amplification of surface Ca^{2+} influx and regulation of neural secretion.

endoplasmic reticulum | ryanodine receptor | exocytosis

Ca^{2+} is a ubiquitous intracellular messenger that regulates vital physiological processes ranging from synaptic transmission, muscle contraction, hormone secretion to cell survival, and cell death (1–3). In neurons, as in other types of cells, the cytoplasmic Ca^{2+} originates from two sources, Ca^{2+} ingress through voltage- and ligand-gated Ca^{2+} channels in the plasma membrane and Ca^{2+} release from internal stores, mainly the endoplasmic reticulum (ER) (4). Two types of Ca^{2+} channels, namely ryanodine receptors (RyRs) and inositol 1,4,5-trisphosphate receptors (IP$_3$Rs), constitute the pathways for Ca^{2+} release of the ER. The RyR pathway, which operates via the Ca^{2+}-induced Ca^{2+} release (CICR) mechanism, is found in a variety of neurons (5–9), and affords the possibility for excitation-Ca^{2+} release coupling and for generation of Ca^{2+} signal independently of excitation (7).

The Ca^{2+}-dependent vesicular secretion of transmitters and peptides is widely involved in neural, paracrine, and endocrine functions. Most neurons release their neurotransmitters in its terminals at the synapse in a Ca^{2+}-dependent manner. However, Huang and Neher (10) reported that depolarization can trigger capacitance increase in small dorsal root ganglion (DRG) neurons (15–25 μm in diameter, C-type), indicating somatic exocytosis. Using amperometry and imaging technique, we have recently detected quantal release of preloaded transmitters or dyes from the DRG somata in response to action potentials (11, 12). Among others, pain-related peptides such as calcitonin gene-related peptide (CGRP) and substance P may be released from the somata of the cell (13, 14). Thus, the somatic secretion most likely provides a way for an excited DRG neuron to modulate the activity of adjacent ganglion neurons (including itself) and thereby the transmission of sensing and nociceptive inputs to the spinal cord and higher central nervous system (CNS).

To trigger exocytosis, local Ca^{2+} must exceed several (in chromaffin cells) or 10 micromolar (in terminals) (15), and such high concentrations can only be achieved in the vicinity of a Ca^{2+} channel. Intriguingly, in many vertebrate and invertebrate neurons of both the CNS and peripheral systems, including DRG, specialized regions of the ER, dubbed subsurface cisternae (SSC), come into direct apposition to the plasma membrane, forming nanoscopic junctions reminiscent of the dyads or triads in muscles (16, 17). At places of SSC, Ca^{2+} release might occur spontaneously or it can be coupled to local Ca^{2+} entry via the CICR mechanism and, consequentially, elevate local Ca^{2+} concentrations to trigger exocytosis of nearby vesicles.

In the present study, we investigated local Ca^{2+} signaling between surface membrane and SSC and its role in the regulation of secretion in DRG sensory neurons. In particular, we demonstrated that Ca^{2+} release from type 3 RyRs on SSC, in the form of "Ca^{2+} sparks" (18), can occur spontaneously or provoked by caffeine and its analog 3,7-dimethyl-1-(2-propynyl)xanthine (DMPX). During excitation, similar sparks are triggered by and amplify the surface Ca^{2+} influx. These subsurface sparks play an important role in triggering and modulating vesicular secretion from the somata of DRG neurons.

Methods

Cells and Patch Clamp Recordings. Freshly isolated rat DRGs (C5–L5) were prepared with collagenase (1.5 mg·ml^{-1}) and tripsin (1 mg·ml^{-1}) at 37°C, as described (11). Cells were used 1–10 h after preparation. Only the small (15–25 μm, C-type) neurons without apparent processes were used. Whole-cell patch-clamp recordings were performed in either perforated or broken-in configuration by using an EPC9/2 amplifier and PULSE software (HEKA Elektronik, Lambrecht/Pfalz, Germany). Standard external solution contained 150 mM NaCl, 5.0 mM KCl, 2.0 mM CaCl$_2$, 1.0 mM MgCl$_2$, 10 mM Hepes, and 10 mM glucose, at pH 7.4. The patch pipette (2–4 MΩ) filling solution contained 150 mM CsCl, 4.0 mM MgCl$_2$, 10 mM Hepes, and 0.15 mM nystatin (omitted in the broken-in configuration), at pH 7.2. All experiments were performed at room temperature (22–25°C).

Ca^{2+} Imaging. DRG neurons were loaded with fluo-4 AM (5 μM, 30 min) (Molecular Probes), and imaged with a Zeiss 510 inverted

PHYSIOLOGY

confocal microscope with $\times 40$ oil immersion lens (numerical aperture 1.3). The horizontal and axial resolutions were 0.4 and 1.5 μm, respectively. Line scan, curve scan, and 2D imaging modes were used to measure sparks and Ca^{2+} transients. Extracellular solution contained 150 mM NaCl, 5.0 mM KCl, 1.1 mM $MgCl_2$, 10 mM glucose, 10 mM Hepes, and 2.0 mM $CaCl_2$ (pH 7.4). In some experiments, caffeine or DMPX was added to nominal zero Ca^{2+} solution and delivered to cells by locally placed glass pipette. Image processing and data analysis were performed by using IDL 5.4 software (Research Systems, Boulder, CO). Automated detection and analysis of sparks used the computer algorithm developed by Cheng *et al.* (19). Fitting the spatial and temporal profiles of sparks used the procedure described in refs. 20 and 21.

Membrane Capacitance (C_m) Measurement. The C_m was measured with standard whole-cell patch-clamp configuration by using the software lock-in module of PULSE 8.30 together with an EPC9/2 amplifier. A 1-kHz, 40-mV peak-to-peak sinusoid was applied around a DC holding potential of -80 mV. The resulting current was analyzed by using the Lindau–Neher technique to give estimates of the C_m, membrane conductance, and series resistance (22). Patch pipette (2–3 MΩ) filling solution contained 150 mM CsCl, 5.0 mM MgATP, 0.1 mM Li_4GTP, 10 mM Hepes, and 0.25 mM fluo-4 or 0.1 mM fura-2 potassium salt. Voltage commanding pulses were synchronized to confocal imaging by marking the image with a 1-ms LED flash at the onset of the C_m recording.

RIA of CGRP Release. DRG neurons were enzymatically isolated from neonate rats as described (23). Cells were maintained in culture for $\approx$3–6 days before CGRP release assay. After washing with DMEM, cultured DRG neurons were incubated in 1 ml of DMEM, to measure the basal release of CGRP, or in DMEM containing designated reagents. After 20-min incubation, the supernatants were removed from the culture wells, and the amounts of CGRP-like immunoactivity (LI) were measured with use of CGRP RIA as described (24).

Immunolabelling. Dissociated DRG neurons were fixed and incubated overnight with primary monoclonal antibodies that recognize RyR2, RyR1,2 (both RyR1 and RyR2), and RyR1,3 (both RyR1 and RyR3) (25) at 4°C, then incubated with Cy3-conjugated anti-mouse antibodies (Jackson ImmunoResearch) for 1.0 h in the dark.

Statistics. Data were given as mean $\pm$ SEM. The significance of difference between means was determined, when appropriate, by using nonparametric Kruskal–Wallis test, Student's t test, and paired t test. $P < 0.05$ was considered statistically significant.

Results

Ca^{2+} Sparks in DRG Neurons. Small sensory neurons from rat DRGs were examined with confocal microscopy in conjunction with the Ca^{2+} indicator, fluo 4, under conditions conducive to CICR (1 mM caffeine to sensitize RyRs). Time-lapsed confocal imaging revealed sudden, local, and short-lived elevations of the cytoplasmic Ca^{2+}, namely Ca^{2+} sparks, at the periphery of the cell body (Fig. 1*A*). High-resolution line scan imaging along the cell diameter showed that individual sparks remain highly confined in space and time, with no incidence of activating regenerative Ca^{2+} waves (Fig. 1*B*). DRG sparks were abolished by RyR antagonists, ryanodine at a high concentration (10 μM for 20 min, $n = 15$ cells; Fig. 1*B*), and tetracaine at 1 mM ($n = 6$ cells), indicating the RyR origin of sparks. However, DRG sparks could not be prevented by the IP_3R antagonist xestospongin C (10 μM, 10 min, $n = 11$ cells) or 2-aminoethoxydiphenyl borate (2-APB, 20 μM, 10 min, $n = 10$ cells). Although 2-APB at high concentrations (50–100 μM) blocks also the store-operated Ca^{2+} entry (26), these data collectively suggest that IP_3Rs are not required for the genesis of sparks in DRG
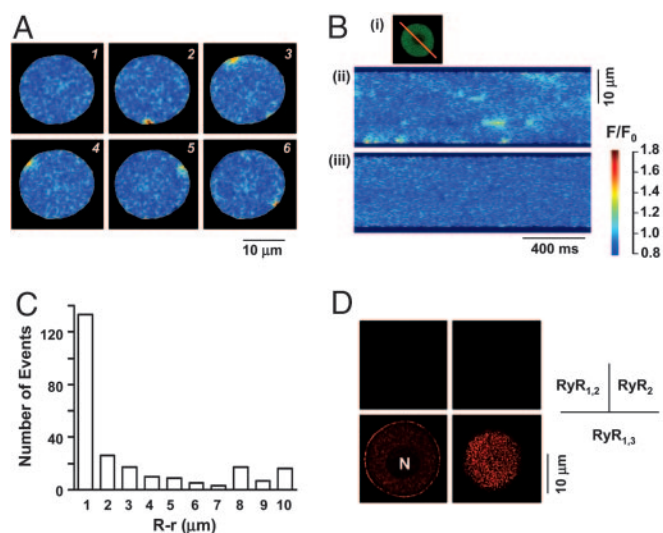

Fig. 1. Ca^{2+} sparks in DRG neurons. (*A*) Sequential confocal images of a DRG neuron in the presence of 1 mM caffeine. Images were taken 0.25 s apart. (*B*) Ca^{2+} sparks along the cell diameter (*ii*) and their inhibition by ryanodine (10 μM, 20 min) (*iii*). (*i*) Scan line position. (*C*) Radial distribution of sparks, $f(R - r)$, where R is the radius of the cell and ($R - r$) is the distance from surface. The number of sparks in a shell (r) should be proportional to $4\pi r^2 f(R - r)$, and $\approx$75% of sparks were restricted to the 1-μm outermost shell. (*D*) Subsurface localization of RyR3 immunofluorescence. No specific immunoreactivity was observed for anti-RyR1,2 and anti-RyR2 antibodies (*Upper*). (*Lower Right*) The punctuated RyR3 immunofluorescence on cell surface flattened by a coverslip.

neurons. Furthermore, DRG sparks persisted upon brief removal of external Ca^{2+} ($n = 8$ cells), excluding Ca^{2+} influx as the direct source of Ca^{2+}.

Subsurface Localization of DRG Sparks. Mapping the spark-igniting sites uncovered a striking subsurface localization of DRG sparks. Of 238 sparks observed along the diameter of DRG cells, 133 (56%) were found within 1 μm of the surface (Fig. 1*C*). Considering the spherical geometry of the cell body, we estimated that $\approx$75% sparks are localized to the outmost 1-μm shell of the cytoplasm (Fig. 1). To determine the subcellular organization of RyRs participating in the genesis of sparks, we performed immunocytochemical assay using antibodies reacting with different RyR isoforms. Our data showed the presence of type 3, but neither type 1 nor type 2 RyR reactivity in DRG cells (Fig. 1*D*), in agreement with a recent report (27). RyR3 immunofluorescence was sharply enriched at punctuated sites, and such "puncta" were seen most abundant along a shell immediately beneath the cell surface (Fig. 1*D*). By focusing on the coverslip-flattened cell surfaces, we estimated the density of subsurface RyR3 to be 0.33 sites per μm^2 (Fig. 1*D*). Tissue staining of entire ganglions further revealed that almost all neurons are equipped with such subsurface RyR3 puncta (data not shown).

It was shown in early 1960s that, in many types of neurons including DRG cells, SSC make contacts with the plasma membrane at the somata and proximal processes (16), but their physiological significance remains elusive. In this regard, the aforementioned functional and immunocytochemical data strongly suggest that SSC represent the Ca^{2+} release units that give rise to sparks in DRG neurons. These uniquely placed subsurface sparks from RyR3 on SSC might be instrumental to reciprocal communication between the plasma membrane and the intracellular Ca^{2+} stores.

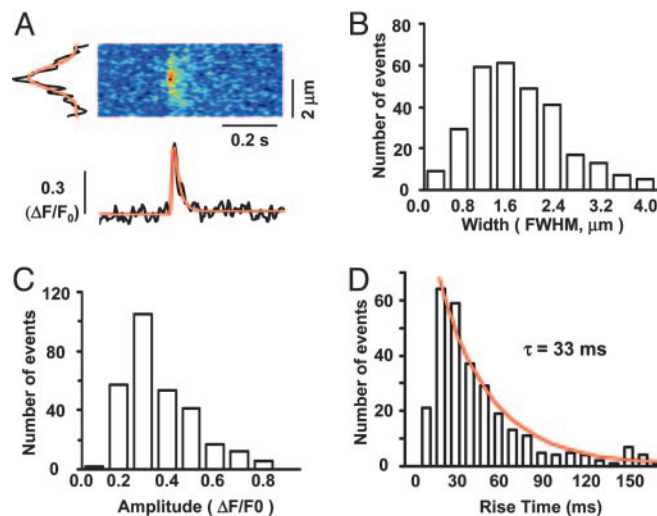**Triggering Sparks by Physiological Ca^{2+} Entry.** Given the subsurface localization of RyR3 and sparks, it is possible that membrane excitation of DRG cells is coupled to spark production, translating neural activity into intracellular Ca^{2+} signal. To investigate the
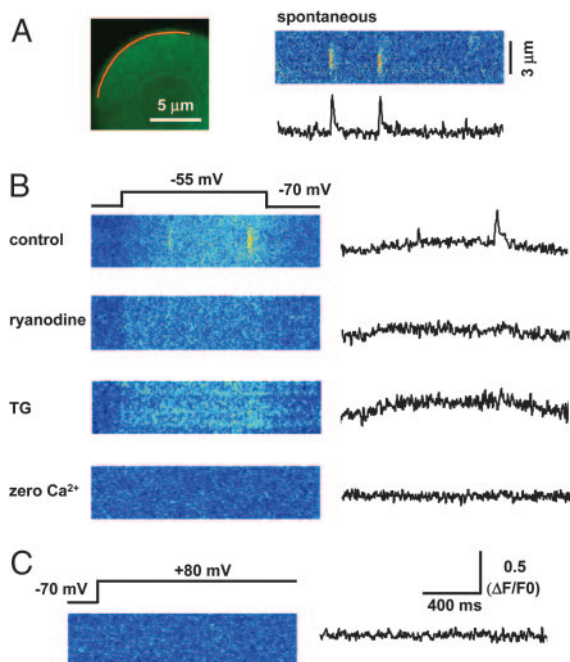
Fig. 2. Depolarization-evoked sparks. (*A*) Spontaneous sparks in the absence of caffeine. (*Inset*) Confocal curved line scan (red) at a repetition rate of 330 Hz. (*B*) Small depolarization activated subsurface sparks under the perforated whole-cell patch clamp conditions. Ryanodine (10 μM) or thapsigargin (TG, 10 μM) or removal of extracellular Ca^{2+} (*Lower*) abolished depolarization-induced sparks. (*C*) Depolarization to the apparent reversal potential of Ca^{2+} currents (+80 mV) failed to elicit any sparks.

Fig. 3. Properties of neuronal Ca^{2+} sparks. (*A*) A typical spark obtained in the presence of 1 mM caffeine. (*B–D*). Histograms of spark amplitude (*B*), width (*C*), and release duration (from the onset to the beginning of decay) (*D*). Exponential fit (smooth curve) to the data in *D*, excluding the first data point, yielded a time constant (τ) 33.2 ms.

hypothetical excitation–spark coupling, we used the "curve scan" imaging technique in which the scanning laser beam tracks a curved trajectory underneath the cell surface (Fig. 2*A Inset*). Subsurface sparks in the absence of caffeine occurred at a rate of 0.40 ± 0.16 $(100\ \mu m)^{-1} \cdot s^{-1}$ ($n = 18$ cells; Fig. 2*A*), whereas 1 mM caffeine increased the spark rate to $10.3 \pm 0.8\ (100\ \mu m)^{-1} \cdot s^{-1}$ ($n = 41$ cells, $P < 0.01$ vs. control). Fig. 2*B Top* illustrates that, in a voltage-clamped cell, near-threshold depolarization from holding potential -70 mV to -55 mV evoked sparks amidst an elevating Ca^{2+} background [$1.58 \pm 0.46\ (100\ \mu m)^{-1} \cdot s^{-1}, n = 15$ cells, $P < 0.05$ vs. control]. The depolarization-evoked sparks were indistinguishable from the spontaneous sparks in the absence of caffeine (Fig. 2*A*), and were abolished by ryanodine [$0.03 \pm 0.03\ (100\ \mu m)^{-1} \cdot s^{-1}, n = 17, P < 0.01$ vs. untreated cells] or thapsigargin pretreatment [$0.04 \pm 0.04\ (100\ \mu m)^{-1} \cdot s^{-1}, n = 8, P < 0.05$ vs. untreated cells; Fig. 2*B*]. However, the dim and homogenous Ca^{2+} background was ryanodine- and thapsigargin-resistant (Fig. 2*B*), consistent with the notion that it arises from voltage-gated Ca^{2+} currents (I_{Ca}), such as those of L- N-, P-, and Q-type high voltage-activated and T-type low voltage-activated Ca^{2+} channels in the plasma membrane (28, 29). Depolarization in the absence of extracellular Ca^{2+} (Fig. 2*B*; $n = 10$ cells) or to the apparent reversal potential of I_{Ca} (+80 mV, Fig. 2*C*; $n = 12$ cells) failed to elicit any increase in local sparks or background Ca^{2+} elevation. These findings indicate that Ca^{2+} entry via I_{Ca}, rather than the membrane depolarization per se, is obligatory to ignition of sparks during excitation. Taken together, we conclude that DRG sparks are coupled to membrane excitation by the CICR mechanism.

Unitary Properties of DRG Sparks. The unitary properties of DRG sparks were measured by fitting the spatial profiles, the rise and decay time courses of individual sparks to Gaussian and monoexponential functions (Fig. 3*A*). We found that there is a decaying distribution for spark amplitude (Fig. 3*B*) and a bell-shaped distri-

bution for spark spatial width (Fig. 3*C*). The release duration of DRG sparks followed a monoexponential distribution (time constant $\tau = 33.2$ ms; Fig. 3*D*), as if DRG spark termination is governed by a first-order stochastic process. Notably, many DRG spark-igniting sites manifested repetitive activity (Figs. 1 and 2), suggesting that DRG spark production exhibits little use-dependent refractoriness.

Regardless whether they were spontaneous events or caffeine- or depolarization-evoked ones, DRG sparks displayed similar amplitudes ($\Delta F/F_0 = 0.27 \pm 0.05$, 0.32 ± 0.01 and 0.33 ± 0.01, $n = 13$, 293, and 40 for spontaneous, caffeine-, and depolarization-evoked events, respectively), spatial spread (full width at half maximum = 2.03 ± 0.29, 2.05 ± 0.05 and $1.98 \pm 0.26\ \mu m$), and release duration (37.9 ± 6.3, 45.9 ± 2.6 and 47.5 ± 7.7 ms). The similarities of DRG sparks under various experimental conditions support the notion that sparks constitute the elementary Ca^{2+} release events in DRG neurons. That caffeine increases the propensity of spark occurrence without affecting their unitary properties suggests that caffeine specifically modulates the activation, but not termination, of the elementary release events in DRG neurons.

DRG Sparks Directly Trigger Exocytosis. Because the vast majority of sparks are precisely localized to the membrane subspace (Fig. 1), it is tempting to speculate that subsurface sparks are involved in regulating the release of vesicles in their immediate vicinities. Next, we sought to test this possibility by measuring C_m during store Ca^{2+} release. Because C_m is proportional to the surface area of the cell, stimulus-induced capacitance increase (ΔC_m) provides a sensitive measurement of vesicle fusion in somata of DRG neurons (10). This fusion is thought to be a key event for delivering the bioactive cargos (e.g., CGRP and substance P) into the extracellular space to affect possible autocrine and paracrine functions. Caffeine or its analog, DMPX, at 5 mM in Ca^{2+}-free solution evoked a large number of discrete sparks that were quickly fused into global Ca^{2+} transients (Fig. 4 *A* and *C*). The average transient amplitude were $\Delta F/F_0 = 1.33 \pm 0.13$ (caffeine, $n = 8$) or 1.43 ± 0.15 (DMPX, $n = 13$), respectively. Assuming that sparks constitute the building blocks of the global Ca^{2+} transients and based on unitary properties of sparks, we estimated that an average subsurface Ca^{2+} transient induced by 5 mM caffeine or DMPX is equivalent to the summation of 1,582 or 1,701 subsurface sparks (Fig. 4*D*), respectively.

PHYSIOLOGY
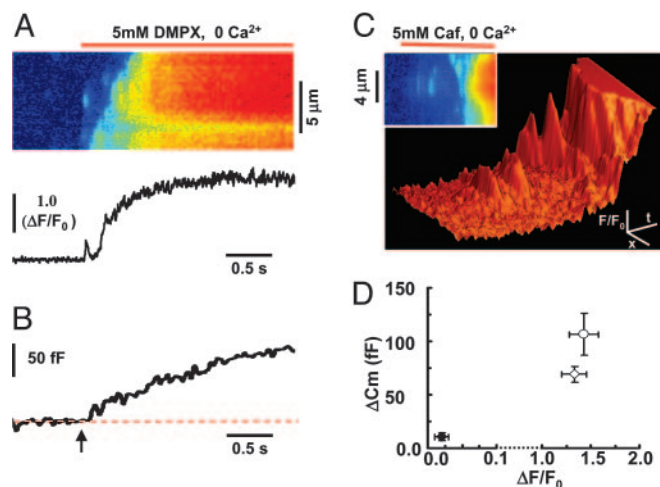
Fig. 4. Ca^{2+} sparks and secretion in DRG neurons. (*A* and *C*) Ca^{2+} sparks as the building blocks of caffeine- and DMPX-induced global Ca^{2+} transients. Curve scan imaging was performed as in Fig. 2. DMPX (*A*) and caffeine (*C*) at 5 mM elicited sparks quickly fused into globe Ca^{2+} transients. An expanded vertical scale was used in *C* to highlight the leading sparks, rendering the flattened top because data are out of scale. (*B*) ΔC_m responses to 5 mM DMPX. Arrow denotes the application of DMPX. (*D*) Relationship between peak Ca^{2+} transients ($\Delta F/F_0$) and ΔC_m (measured 3 s after caffeine or DMPX application). The equivalent number of subsurface sparks $N = (\Delta F/F_{0,CT} \times 4\pi r^2)/(\Delta F/F_{0,sk} \times \pi W^2/4)$, where $\Delta F/F_{0,CT}$ refers to the peak Ca^{2+} transient, r (=10 μm) is the radius of a typical cell, and $\Delta F/F_{0,sk}$ (=0.32) and W (=2.05 μm) are the peak and the full width at half maximum of a spark, respectively. Filled diamonds, thapsigargin pretreatment (10 μM 20 min), 5 mM caffeine; open diamonds, 5 mM caffeine; open circles, 5 mM DMPX. $n = 5$–14 for each data point.

Fig. 4*B* shows typical time course of C_m change measured in cells free of Ca^{2+} indicator under otherwise identical conditions. On average, we detected a ΔC_m of 69.9 ± 7.5 fF ($n = 14$) at 5 mM caffeine, and 107.7 ± 20.0 fF ($n = 6$) at 5 mM DMPX (Fig. 4*D*), which corresponds to the secretion of ≈140 and 215 vesicles (assuming 1 fF = 2 vesicles) (11), respectively. Inhibiting the ER Ca^{2+} pump by thapsigargin virtually abolished the Ca^{2+} and ΔC_m responses to 5 mM caffeine (Fig. 4*D*). Thus, we conclude that spark-mediated store Ca^{2+} release stimulates vesicle secretion independently of membrane excitation and Ca^{2+} influx. Given the above estimates of the equivalent number of sparks (see above), we further inferred the spark-secretion coupling probability to be one vesicle per 11.3 or 7.9 sparks in response to 5 mM caffeine or DMPX, respectively.

The spark-secretion coupling probability was further determined on the basis of the C_m rising slope and the rate of spark occurrence in indicator-loaded cells exposed to 1 mM caffeine (Fig. 5*A*). Under these experimental conditions, the rising rate of C_m was 4.9 fF·s^{-1} (data from 41 cells, Fig. 5*B Upper*), i.e., ≈9.8 vesicles per s in a cell. Concomitantly, the spark rate of occurrence was 10.3 (100 μm)$^{-1}$·s^{-1} (data from 41 cells) as seen in the curve scan images (Fig. 5*B Lower*). Assuming that curve scan imaging registers sparks within a 2-μm zone centered at the line, the spark rate of occurrence in a cell of 20 μm diameter should be 65 sparks per s on the entire subsurface shell. These numbers led to an estimate of the coupling probability to be one vesicle per 6.6 sparks in 1 mM caffeine.

Next, we sought to resolve whether any C_m changes coincided with individual sparks. For this, confocal imaging and C_m recording were precisely synchronized by marking the image with a 1-ms LED flash lit at the onset of C_m recording. We recorded a large quantity of sparks with the corresponding C_m noise below a selection criterion (<35 fF at 1.24-ms resolution). They were then aligned and signal-averaged by using the onset of solitary sparks or the onset of the first sparks in bursting events (Fig. 5*A*) as the guide. The
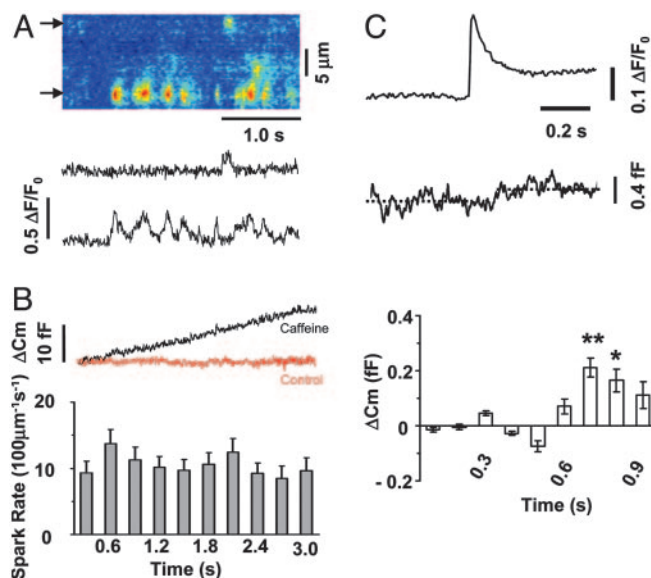
Fig. 5. Spark-secretion coupling. (*A*) Spark response to 1 mM caffeine. Time courses of solitary or bursting sparks at marked sites are shown beneath the image. (*B*) Simultaneously recorded C_m (line plot) and spark production (bar graph) in 1 mM caffeine. C_m traces of 3-s length from 41 cells were averaged and shown on the top, with control traces obtained from the same cells before caffeine application. Linear fitting to the average C_m trace in caffeine yielded a slope factor of 4.9 fF·s^{-1}. (*C*) C_m changes associated with individual sparks. (*Top*) Total of 897 traces with a spark event starting at $t = 400$ ms were aligned and averaged by using the spark onset as the guide. The trailing plateau of the averaged trace was due to bursting spark activity (*A* and Figs. 1 and 2). (*Middle*) To reveal specific C_m signal linked to the average spark, the linear rising C_m component was estimated from the data 0–400 ms before the sparks and was then subtracted from the averaged C_m trace. Dashed lines mark the levels 0–400 ms before and 100–500 ms after the onset of the average spark, respectively. (*Bottom*) Statistics of ΔC_m at 100-ms intervals. **, $P < 0.01$; *, $P < 0.05$ vs. control (0–400 ms before the spark).

average results of 897 spark–C_m pairs from 41 cells are shown in Fig. 5*C*. Because of the frequent bursting spark activity, the average spark displayed an early peak followed by a sustained plateau (Fig. 5*C Top*); its signal integral (0–500 ms from the onset) was equivalent to those of 2.2 solitary sparks. Importantly, we uncovered a small but significant C_m increase associated with the average spark (0.14 ± 0.03 fF between 100–500 ms after the onset of the spark; $P < 0.01$ vs. 0.0 ± 0.03 fF between 0–400 ms before the spark; Fig. 5*C Middle*). As a control, we detected no significant changes on randomly chosen C_m traces (i.e., not aligned to specific spark events) in 1 mM caffeine ($n = 812$, data not shown). These measurements not only substantiate the notion on spark-mediated vesicle release, but also suggest the coupling probability to be approximately one vesicle per 7.9 sparks. It is noteworthy that a significant increase in C_m was first detected with a latency of ≈200 ms (Fig. 5*C Bottom*), suggesting that the spark-mediated vesicle fusion is of slow kinetics or involves multiple intermediate steps.

Store Ca^{2+} Release Modulates Excitation–Secretion Coupling. Neural secretion is a superlinear function of Ca^{2+} concentration (30, 31), implicating a possible synergism between sparks and Ca^{2+} entry in controlling exocytosis. To appraise this possibility, we measured depolarization-induced vesicle secretion in the absence and presence of a RyR antagonist (whole-cell dialysis of 50 μM ryanodine). Under whole-cell patch-clamp conditions, 200-ms depolarization to 0 mV induced 460 ± 200 fF ΔC_m ($n = 6$, Fig. 6*A Left*). After 11-min recording without ryanodine dialyzed into the cell, same depolarization induced a ΔC_m that was reduced by 50% (due to run down) (Fig. 6*A Left*). By contrast, such depolarization-induced ΔC_m was
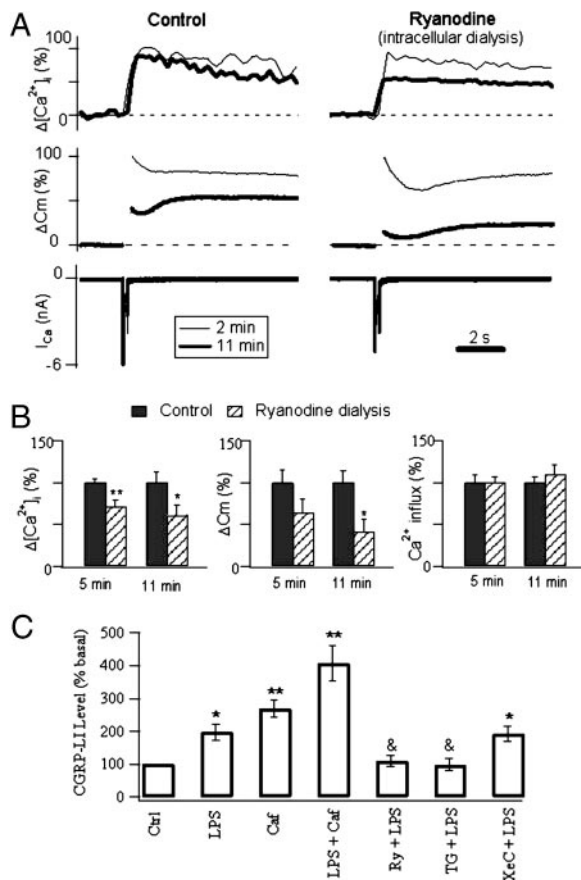
Fig. 6. Ca^{2+} sparks contribute to depolarization- and endotoxin-induced exocytosis and neuropeptide secretion. (*A*) Intracellular dialysis of ryanodine (Ry, 50 μM) caused smaller $[Ca^{2+}]_i$ transients and greatly reduced ΔC_m during depolarization (200 ms, −80 mV to 0 mV). ΔC_m was measured at 2 and 11 min after whole-cell dialysis with or without ryanodine. $[Ca^{2+}]_i$ transients ($\Delta[Ca^{2+}]_i$) were expressed as the percent of that at 2 min. (*B*) Statistical analysis. Data were expressed as the percent of the control values at the same time point. Ryanodine dialysis for 5 or 11 min decreased Ca^{2+} transients and ΔC_m, but not the I_{Ca}. $n = 6$ for each group; **, $P < 0.01$; *, $P < 0.05$ vs. the corresponding control. (*C*) CGRP release in cultured neonatal DRG neurons. The basal level of CGRP-like immunoactivity (CGRP-LI) was 48.2 ± 6.7 pg·ml^{-1}. Caffeine (Caf, 3 mM) potentiated LPS-stimulated (1 μg·ml^{-1}) CGRP release, whereas thapsigargin (TG, 10 μM) and ryanodine (Ry, 10 μM), but not xestospongin C (XeC, 12 μM), suppressed the LPS-induced CGRP release. $n = 5$–8 independent experiments. **, $P < 0.01$; *, $P < 0.05$ vs. control (ctrl); &, $P < 0.05$ vs. LPS alone.

reduced by ≈90% of the initial value in the presence of intracellular 50 μM ryanodine (Fig. 6*A Right*). Compared to control values at 11 min, ryanodine caused a 44% reduction in Ca^{2+} transient amplitude ($P < 0.01$) without affecting I_{Ca} (Fig. 6*B*), and inhibited vesicular secretion by 60% ($P < 0.01$) because of the nonlinear relation between $[Ca^{2+}]_i$ and secretion. These results indicate that spark-mediated release acts in synergy with Ca^{2+} influx in the modulation of excitation–secretion coupling.

Inhibition of Sparks Prevents Endotoxin-Induced CGRP Release. Secretion in DRG cells not only is linked to membrane electrical activities, but also is modulated by receptor-mediated signal transduction. For instance, we have recently shown that lipopolysaccharide (LPS), known also as endotoxin, stimulates the release of CGRP, a 37-aa pain-related neuropeptide, from neonatal rat DRG neurons in culture (23). Using a RIA, we examined the possible involvement of CICR production in the endotoxin-induced CGRP secretion (Fig. 6*C*). We found that incubation with 3 mM caffeine

caused a significantly elevated CGRP release and potentiated the CGRP release in response to endotoxin. Conversely, inhibition of RyRs or ER Ca^{2+}-ATPase abolished the LPS-induced CGRP secretion, whereas selective inhibition of IP_3Rs with xestospongin C (12 μM) exerted no significant effect. These findings suggest that RyR-mediated release is required for endotoxin-induced neuropeptide secretion.

Discussion

Neural Ca^{2+} Sparks. In the present study, we have provided an unequivocal demonstration of sparks as the elemental store Ca^{2+} release events in a mammalian sensory neuron. Arising from RyR3 mostly on SSC, these sparks occur spontaneously at a low frequency in resting DRG cells, but can be readily activated with the RyR sensitizers, caffeine and DMPX. During excitation, spark production is triggered by physiological Ca^{2+} influx via the CICR mechanism such that the evoked sparks amplify the trigger Ca^{2+} entry, allowing for synergistic interaction between Ca^{2+} release and Ca^{2+} entry in the regulation of local Ca^{2+} signaling events such as exocytosis.

The possibility for the existence of sparks in neurons was first suggested on the basis of excessive "noise" or bright pixels revealed by histogram analysis of neuronal Ca^{2+} images in which no discernible local events could be resolved (32). Meanwhile, Koizumi *et al.* (33) showed that, in nerve growth factor-differentiated PC12 cells or cultured hippocampal neurons, the elementary Ca^{2+} release events arise from both RyR and IP_3R, and exhibit 2-fold greater spatial width and at least 20-fold longer duration than a typical cardiac spark. Later, Llano *et al.* (7) visualized RyR-mediated spontaneous Ca^{2+} release at presynaptic terminals, where individual events last for a few seconds and spread by 5–10 μm along the processes. These local Ca^{2+} release events along neural process might involve CICR among multiple release sites and therefore reflect compound Ca^{2+} sparks. Most recently, local Ca^{2+} release events called Ca^{2+} syntillas have been characterized at hypothalamic neural terminals with a nonconfocal technique (34). Mechanistically, hypothalamic syntillas can be activated by depolarization in a Ca^{2+}-independent manner, whereas Ca^{2+} influx is obligatory to depolarization-evoked sparks in DRG neurons. Taken together, the recording of Ca^{2+} syntillas and sparks signifies the beginning of investigation of store-mediated Ca^{2+} signaling in neurons on the smallest physiological scale.

Compared to prototypical sparks in muscles ($\Delta F/F_0 \approx 0.7$, full width at half maximum ≈ 2.0 μm, release duration of 5–10 ms), DRG sparks are characterized by a halved amplitude (0.3 $\Delta F/F_0$), similar spatial extension, but markedly prolonged release duration (≈40 ms), displaying a monoexponential distribution. The small amplitude combined with the prolonged release duration predicts that Ca^{2+} release flux underlying a spark must be smaller in DRG neurons than muscle cells. The bursting behavior as well as the long and exponentially distributed release duration make DRG sparks most distinctive, because in striated muscles, tight regulation endows sparks with brief (5–10 ms) and preferred release duration (19, 35) and strong use-dependent inactivation (36, 37). The unique properties of DRG spark termination and refractoriness might stem from the fact that DRG RyR3 in planar lipid bilayers does not inactivate even in the presence of 10 mM Ca^{2+} on the cytosolic side (25).

Spark-Secretion Coupling. The vast majority of DRG sparks are found in 1-μm outmost shell of the cytoplasm, as is the case with RyR3 immunoreactive aggregates. As such, RyR3 sparks are well positioned to mediate reciprocal communication between the plasma membrane and the intracellular Ca^{2+} store. In this regard, we have demonstrated that sparks are directly triggered by local physiological Ca^{2+} entry, and conversely, subsurface sparks are equally well poised to mediate the retrograde signaling, e.g., Ca^{2+}-

dependent vesicular secretion. Multiple lines of evidence have been presented to show role of sparks in triggering and modulating vesicular secretion from somata of DRG neurons. First, activation of sparks by caffeine or DMPX suffices to trigger significant vesicle release indexed by C_m increase. This process requires neither membrane excitation nor Ca^{2+} influx; yet, suppression of spark production by pretreatment with thapsigargin abolishes the caffeine effects. Second, by signal averaging of sparks and the corresponding C_m traces, we were able to resolve a miniscule C_m changes temporally linked to individual solitary or bursting sparks (Fig. 5C). Furthermore, we found that CICR amplifies and works in concert with the Ca^{2+} entry in modulating excitation–secretion coupling. Inhibition of CICR suppresses the major component ($\approx 60\%$) of Ca^{2+}-dependent secretion and abolishes the endotoxin-mediated release of CGRP.

In theory, individual vesicle exocytosis might be coupled to solitary or bursting sparks in a stochastic manner. Indeed, triggering exocytosis by sparks appears to be a probabilistic, rather than deterministic, process. Three different methods were applied to estimate the coupling probability based on the relationship between peak $\Delta F/F_0$ and ΔC_m in response to 5 mM caffeine or DMPX, the relationship between the spark rate and the rising slope of C_m during 1 mM caffeine, and the relationship between averaged individual sparks and the corresponding C_m changes. These estimates fell within a range between one vesicle per 6.6 sparks to one vesicle per 11.3 sparks. This low spark–secretion coupling efficiency is in general agreement with the finding in the CNS synapse calyx of Held, where 10 or more Ca^{2+} channels control the release of a single vesicle (38). The rather long latency (≈ 200 ms) from the onset of the average spark to the first detection of a significant C_m increase, as shown in Fig. 5C, further suggests that multiple steps or slow kinetics underlie the spark-mediated vesicle fusion and secretion.

The demonstration of spark-secretion coupling in DRG neurons

is in general agreement with the observation that CICR contributes to asynchronous exocytosis at frog motor nerve terminals (39). Moreover, it has also been shown that RyR-mediated Ca^{2+} release in presynaptic terminals of basket cells underlie spontaneous, multivesicular secretion, causing large-amplitude miniature inhibitory post synaptic currents in Purkinje cells (7). In hippocampal neurons, CICR has also been shown to modulate synaptic transmission because excitatory postsynaptic potentials are smaller in the presence of ryanodine (9). Collectively, the present and previous findings unveil a role for store Ca^{2+} release in secretion functions at the presynaptic terminals and cell body of neurons. The present finding also sheds light on the long-sought physiological significance of neuronal SSC that forms nanoscopic junctions with the plasma membrane.

In summary, we have demonstrated that sparks arising from RyR3 on SSC underlie excitation-Ca^{2+} release coupling in a mammalian sensory neuron. Owing to their subsurface localization, sparks alone can directly trigger vesicle secretion. When acting in synergy with the surface Ca^{2+} influx, subsurface sparks play an important role in the modulation of excitation–secretion coupling. That RyR inhibition suppresses endotoxin-induced secretion of an excitatory pain-related peptide implicates RyR3 of DRG as a novel target for analgesic therapeutics. These findings, as well as the approaches presented here, may have general implications to understanding store-mediated Ca^{2+} signaling in neuronal activities (transmitter release, somatic secretion, excitability, synaptic plasticity, etc.) at the elementary release level.

1. Clapham, D. E. (1995) *Cell* **80,** 259–268.
2. Neher, E. (1998) *Neuron* **20,** 389–399.
3. Berridge, M. J., Lipp, P. & Bootman, M. D. (2000) *Nat. Rev. Mol. Cell. Biol.* **1,** 11–21.
4. Berridge, M. J. (1998) *Neuron* **21,** 13–26.
5. Llano, I., DiPolo, R. & Marty, A. (1994) *Neuron* **12,** 663–673.
6. Shmigol, A., Verkhratsky, A. & Isenberg, G. (1995) *J. Physiol.* **489,** 627–636.
7. Llano, I., Gonzalez, J., Caputo, C., Lai, F. A., Blayney, L. M., Tan, Y. P. & Marty, A. (2000) *Nat. Neurosci.* **3,** 1256–1265.
8. McDonough, S. I., Cseresnyes, Z. & Schneider, M. F. (2000) *J. Neurosci.* **20,** 9059–9070.
9. Emptage, N. J., Reid, C. A. & Fine, A. (2001) *Neuron* **29,** 197–208.
10. Huang, L. Y. & Neher, E. (1996) *Neuron* **17,** 135–145.
11. Zhang, C. & Zhou, Z. (2002) *Nat. Neurosci.* **5,** 425–430.
12. Zhang, C., Xiong, W., Zheng, H., Lu, B. & Zhou, Z. (2004) *Neuron* **42,** 225–236.
13. Zhang, X., Aman, K. & Hokfelt, T. (1995) *J. Comp. Neurol.* **352,** 481–500.
14. Bao, L., Jin, S. X., Zhang, C., Wang, L. H., Xu, Z. Z., Zhang, F. X., Wang, L. C., Ning, F. S., Cai, H. J., Guan, J. S., et al. (2003) *Neuron* **37,** 121–133.
15. Augustine, G. J. & Neher, E. (1992) *J. Physiol.* **450,** 247–271.
16. Rosenbluth, J. (1962) *J. Cell Biol.* **13,** 405–421.
17. Henkart, M., Landis, D. M. D. & Reese, T. S. (1976) *J. Cell Biol.* **70,** 338–347.
18. Cheng, H., Lederer, W. J. & Cannell, M. B. (1993) *Science* **262,** 740–744.
19. Cheng, H., Song, L. S., Shirokova, N., Gonzalez, A., Lakatta, E. G., Rios, E. & Stern, M. D. (1999) *Biophys. J.* **76,** 606–617.
20. Lacampagne, A., Klein, M. G., Ward, C. W. & Schneider, M. F. (2000) *Proc. Natl. Acad. Sci. USA* **97,** 7823–7828.
21. Hollingworth, S., Peet, J., Chandler, W. K. & Baylor, S. M. (2001) *J. Gen. Physiol.* **118,** 653–678.
22. Lindau, M. & Neher, E. (1988) *Pflugers. Arch.* **411,** 137–146.
23. Hou, L. & Wang, X. (2001) *J. Neurosci. Res.* **66,** 592–600.
24. Mathers, D. A. & Baker, J. L. (1984) *Brain Res.* **293,** 35–47.
25. Airey, J. A., Beck, C. F., Murakami, K., Tanksley, S. J., Deerinck, T. J., Ellisman, M. H. & Sutko, J. L. (1990) *J. Biol. Chem.* **265,** 14187–14194.
26. Bootman, M. D., Collins, T. J., Mackenzie, L., Roderick, H. L., Berridge, M. J. & Peppiatt, C. M. (2002) *FASEB J.* **16,** 1145–1150.
27. Lokuta, A. J., Komai, H., McDowell, T. S. & Valdivia, H. H. (2002) *FEBS Lett.* **511,** 90–96.
28. Abdulla, F. A. & Smith, P. A. (1997) *J. Neurosci.* **17,** 8721–8728.
29. Acosta, C. G. & López, H. S. (1999) *J. Neurosci.* **19,** 8337–8348.
30. Dodge, F. A., Jr., & Rahamimoff, R. (1967) *J. Physiol.* **193,** 419–432.
31. Chow, R. H., Klingauf, J. & Neher, E. (1994) *Proc. Natl. Acad. Sci. USA* **91,** 12765–12769.
32. Melamed-Book, N., Kachalsky, S. G., Kaiserman, I. & Rahamimoff, R. (1999) *Proc. Natl. Acad. Sci. USA* **96,** 15217–152121.
33. Koizumi, S., Bootman, M. D., Bobanovic, L. K., Schell, M. J., Berridge, M. J. & Lipp, P. (1999) *Neuron* **22,** 125–137.
34. Crescenzo, V. D., ZhuGe, R., Velazquez-Marrero, C., Lifshitz, L. M., Custer, E., Carmichael, J., Lai, F. A., Tuft, R. A., Fogarty, K. E., Lemos, J. R., et al. (2004) *J. Neurosci.* **24,** 1226–1235.
35. Rios, E., Shirokova, N., Kirsch, W. G., Pizarro, G., Stern, M. D., Cheng, H. & Gonzalez, A. (2000) *Biophys. J.* **80,** 169–183.
36. Sham, J., Song, L. S., Deng, L. H., Chen-Izu, Y., Lakatta, E. G., Stern, M. D. & Cheng, H. (1998) *Proc. Natl. Acad. Sci. USA* **95,** 15096–15101.
37. Brochet, D. X. P., Yang, D., Di Maio, A., Lederer, W. J., Franzini-Armstrong, C. & Cheng, H. (2005) *Proc. Natl. Acad. Sci. USA* **102,** 3099–3104.
38. Meinrenken, C. J., Borst, J. G. & Sakmann, B. (2002) *J. Neurosci.* **22,** 1648–1667.
39. Narita, K., Akita, T., Osanai, M., Shirasaki, T., Kijima, H. & Kuba, K. (1998) *J. Gen. Physiol.* **112,** 593–609.